# 2013

# Potential damage assessment of a mid-air collision with a small  UAV

Civil Aviation Safety Authority

Civil Aviation Safety Authority / Monash University

12/6/2013

# Revisions

| Date | Name | Notes |
|---|---|---|
| **06.12.2013** | Alexander Radi | Initial version 1.0 |
| | | |

## Executive summary

This report analyses the damage potential to manned aircraft from a mid-air collision with a small unmanned aircraft (UAV). The scenarios of engine ingestion and impacts into fuselage and cockpit windscreen are considered. The aim of the study is to provide velocity estimates, above which penetration of the aircraft structure can be expected. The consequences of the penetration will depend on the impact location, and are not explored in this report.

The method is a combination of reviewing published experimental data and performing original computations using a semi-empirical model. The literature research concentrates on the fields of range safety (RCC, 2007) and uncontained engine failure tests, all of which deal with the penetration of aircraft aluminium plates by compact, fast moving metal fragments. Bird impact studies into windscreens and fuselage were reviewed, but were found of limited value due to the different impact behaviour of organic material compared to components constituting a typical UAV. Assuming that the highest threat of penetration is from the most compact and heavy components of an UAV, a detailed damage analysis of single component impacts (battery pack, motor, payload) was performed using computer simulations (Monte Carlo method).

Literature suggests that ingestion into one engine, and the subsequent thrust loss, is the most likely collision scenario (3 out of 4 cases); the consequences are not likely to be catastrophic, as modern jet aircraft are designed to continue safe flight with one engine loss. For collision velocities above 200kts, UAV parts are predicted to penetrate the fuselage skin, with the potential of damaging internal systems. At landing velocities of large commercial aircraft ($V_{FE}$=160—180kts), penetration of the cockpit windscreen is not likely to occur for small UAVs below 2kg; penetration should be assumed for heavier UAVs. General aviation windscreens will be penetrated at typical cruise velocities, regardless of UAV size/weight.

The equation used for penetration prediction was originally developed for metal plates. Its application to windscreens bears large uncertainties. As no experimental data exist to validate the predictions for windscreen materials, the results should be regarded as rough estimates. It is recommended to commission impact tests of solid objects into windscreen samples.

## Abbreviations

| Abbreviation | Definition |
|---|---|
| **2D** | Two-dimensional |
| **3D** | Three-dimensional |
| **CASA** | Civil Aviation Safety Authority |
| **CASR** | Civil Aviation Safety Regulations |
| **CFR** | Code of Federal Regulations |
| **CS** | Certification Specifications |
| **FAA** | Federal Aviation Administration |
| **FAR** | Federal Aviation Regulations |
| **ft/s** | Feet per second |
| **GA** | General Aviation |
| **kts** | Knots |
| **MPa** | Mega-Pascal ($10^6$ N/m$^2$) |
| **MTOW** | Maximum Takeoff Weight |
| **RMIT** | Royal Melbourne Institute of Technology |
| **UAS** | Unmanned Aerial System |
| **UAV** | Unmanned Aerial Vehicle |
| $V_{50}$ | Ballistic limit velocity |
| $V_C$ | Cruise velocity |
| $V_{FE}$ | Maximum flap extended velocity |

# 1 Table of Contents

# 2   Introduction

## 2.1   Objectives

This report presents the findings of a study carried out by Alexander Radi M.Sc.[1] during a 4 months research internship at CASA (Canberra). The aim of the study is to provide the Standards Development branch at CASA with a potential damage assessment of a mid-air collision between a manned aircraft and a small UAV (MTOW<5kg). The focus is on multi-rotor UAVs ('quad-copters') due their wide spread and availability. The impact into the jet engines, windscreen and fuselage are considered. The work aims to derive critical collision velocities above which UAV components are likely to penetrate into the aircraft interior. The consequences of such penetration are briefly discussed, but their detailed analysis is outside the scope of this report.

## 2.2   Background

Unmanned Aircraft Systems (UAS) is the fastest growing sector of the aviation industry today, with sales expected to top $15 billion by 2014 (RMIT[2]). Nevertheless, a broad range of safety, regulatory, social and technical challenges need to be addressed before the sight of an unmanned aircraft in the sky becomes as common and accepted by the public as its manned counterpart.

Separation, and ultimately collision avoidance ("sense and avoid"), is one of the major technological challenges currently preventing the implementation of the UAS into the controlled airspace. The possibility of a mid-air collision between a conventional aircraft and an UAV is present already today, as limited UAS operations are permitted even without the existence of an effective sense and avoid technology[3]. The consequences of such collisions are not necessarily catastrophic due to the usually low UAV mass, but need to be better understood to assess the overall risk posed by the future increased UAV traffic.

### 2.2.1   Aircraft impact location

The consequences of a mid-air collision with an UAV will strongly depend on the aircraft impact location. Statistics on bird strikes can be used to assess the likelihood of an aircraft part being struck. Figure 1 shows that engine ingestion occurred in 76% of all recorded bird strikes involving transport category aeroplanes, followed by impacts into the windshield with 7%. In general aviation (GA), the windshield is struck in 56% of all cases, followed by the engine.

---

[1] Ph.D. candidate Aerospace Engineering at Monash University, Melbourne
[2] http://www.rmit.edu.au/research/institutes/platformtechnologies/uav
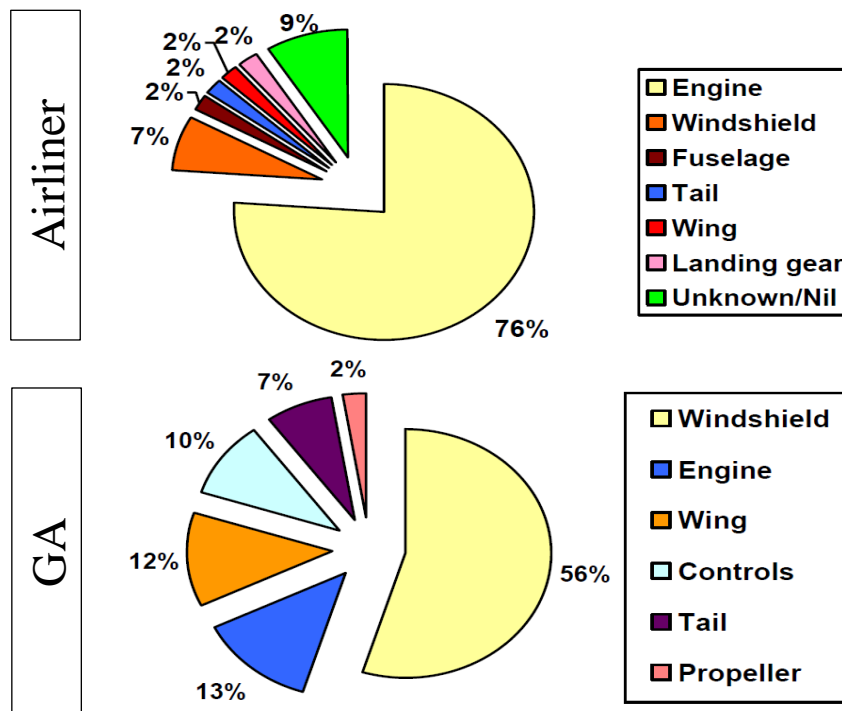[3] CASR 1998, Part 101F

Figure 1: Location of bird strikes for commercial airliners (top) and general aviation (bottom) worldwide for 1912-2011 (Thorpe, 2012).

These data imply that the UAV is most likely to be ingested into one of the jet engines on a commercial airliner, rather than hitting any other aircraft part. The consequences of an engine impact will be discussed in 3. The windscreen penetration is studied in 4.5.

For GA (both fixed and rotary wing), the consequences of a collision are more severe, as the windshield is the most likely part to be struck, and which leads to a fatal outcome in the most cases (Figure 2). The windscreens in this aircraft category are usually made of thin acrylic, and are not required to be able to withstand any bird impact[4]. This lack of design requirements puts the pilot and passengers at high risk, as already a 40g bird can penetrate the windscreen (Thorpe, 2012). In addition, avoidance manoeuvres of general aviation pilots have led to fatal crashes in the past, something that is a possibility during an encounter with an airborne UAV. Section 4.5.3 shows that for GA category, penetration of the windscreen is predicted in all cases at cruise velocity.
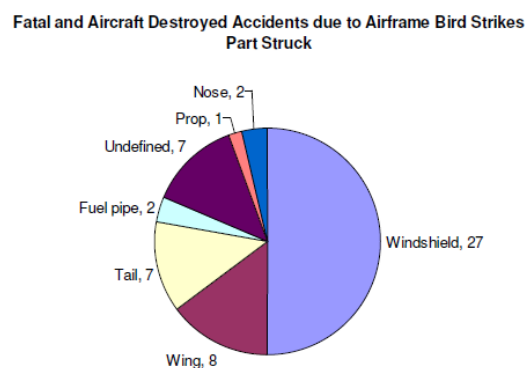


Figure 2: Parts struck during non-engine bird strike accidents (GA aircraft) (ATKINS, 2008).

---

[4] Under FAR-23 and CS-23, only the windscreens of the commuter category are required to withstand an impact of a 2lb bird at maximum approach flap speed [FAR § 23.775(h)(1)].

# 3 Engine ingestion

As discussed in the previous section, engine ingestion is the most often reported type of bird strike for commercial airliners (76%), followed by windscreen damage. The predominance of engine impacts is rather surprising, as the engine capture area (cross-sectional area of the airstream into all engines) is only 2—4% of the overall frontal area of a turbofan aircraft (Cole, et al., 1997). Nevertheless, the same probability will be assumed for the UAV impact, which means that 3 out of 4 occurrences should result in ingestion of the UAV.

The consequences of the ingestion depend on whether the foreign object enters the engine core or by-passes it. Only a part of the air processed through a turbofan engine actually goes through the engine core, which contains the compressors, burners and turbines. The rest passes only through the fan; the bypass ratio of modern engines can exceed 8. In general, the greater the bypass ratio is, the smaller the chance that an object will enter the engine core (Cole, et al., 1997).

**Figure 3: Modern turbofan engine with a high bypass ratio.**

In any case, substantial damage to the fan blades should be expected. Even the ingestion of a bird, which behaves like a fluid at high impact velocities, results in large blade deformations (Figure 4). Although certification standards require the engines to tolerate the impact by birds of a certain size[5], and the involved impact physics are being studied in detail (Vignjevic, et al., 2013), no experimental studies could be found on the consequences of the ingestion of solid objects.
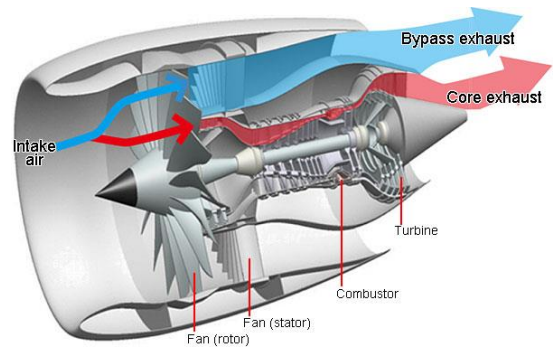
This CRJ600 with 20 passengers on board ingested doves into #1 engine at rotation from a southern USA airport. The engine sustained substantial damage and the aircraft was forced to make a precautionary landing.

**Figure 4: Fan blade damage from bird strike (Cleary, et al., 2006).**

---

[5] EASA Airworthiness Code CS-E 800 'Bird Strike and Ingestion'; corresponding FAA requirements are given in CFR Part 33

The most likely consequence of solid object ingestion is the partial or total loss of engine thrust. This can be expected for metal objects as light as 1g entering the engine core (Cole, et al., 1997) (RCC, 2007). This foreign object ingestion can be accompanied by the throw of fan blade fragments or compressor blades, with subsequent penetration of other aircraft parts.

The danger to the aircraft from such events is solely based on past experiences of uncontained engine failure and expert opinions. (Wilde, 2010) quotes FAA experts and guidelines, stating "that debris ingestions into commercial aircraft engines are unlikely to generate a potentially catastrophic condition due to engine fragment throw. Specifically, the experts reported that (1) engine ingestion of a fragment less than 300 grams is unlikely to produce uncontained impacts other than perhaps some fan blade fragments, (2) experience shows that uncontained fan blade impacts have the potential to impact the fuselage, causing injury, significant damage to the plane, or decompression, but (3) this is less than a 1 in 100 occurrence".

It can be assumed that the loss of one engine will not result in a catastrophic failure. Current law for commercial transport aircraft requires designs that enable continued safe operation following any single engine loss (14 CFR §25.903(b)). Empirical data indicates about one out of a thousand engine losses results in a catastrophic outcome (Wilde, 2010).

The conclusion for the present study is that an ingestion of the UAV into one of the engines is the most likely event, but which is unlikely to result in in a catastrophic outcome.

# 4  Impact damage

Besides ingestion into the engine, the collision of the UAV with the remaining frontal area of an aircraft can result in parts of the UAV penetrating into the interior of the aircraft structure. The consequences of penetration will depend on the impact location, and can include, but are not limited to: damage of electrical or hydraulical systems or other control systems, penetration of the fuel tank, weakening of the structural elements (stringers, spars) or injury/fatality of crew members or passengers.

## 4.1  Bird impacts

One way to assess the damage potential of UAV impacts into the fuselage and windscreen is to analyse past occurrences and studies of bird impacts. Bird impacts into the fuselage can result in substantial local damage (Figure 5), and can potentially lead to catastrophic consequences if the windscreen is penetrated. Fuselage collisions with birds up to 4lb mass are covered by FAR-25, which requires the "continued safe flight and landing after impact with a 4lb bird at cruise speed ($V_C$) at sea level or $0.85V_C$ at 8000ft (2438 m), whichever is the most critical". The same requirement applies to windshields and supporting structure, which "are to withstand the above impact without penetration or critical fragmentation".



Figure 5: Damage to a Boeing 747 flap after a bird collision at 1200 feet AGL (Cleary, et al., 2006).

It appears questionable that the collision with a rigid UAV is comparable to the impact of a 'soft' bird. Birds, and organic materials in general, behave like fluids during a high-speed impact. Figure 6 shows the flowing behaviour of a simulated bird during an impact into a flap section at 194kts. The disintegration and the flowing of the bird absorb energy, which decreases the impact forces. A non-deformable impactor, such as an UAV component, creates a localized strain field in the target material with high peak forces, which supports a 'plugging' as material failure mode. The high peak forces are likely to result in penetration at lower impactor masses compared to birds. This report will assume non-deformable impactors with a plugging penetration mode.
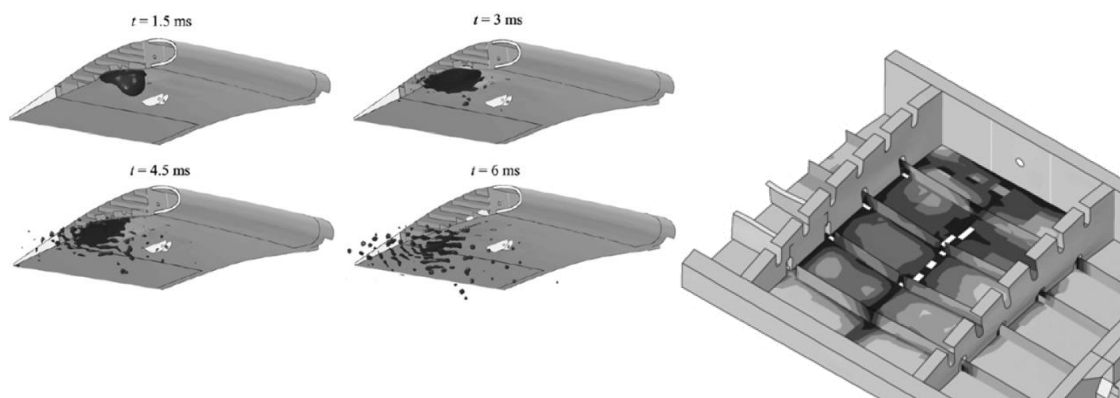


Figure 6: Impact of a 4lb bird into an extended flap at 100m/s (194kts) (Smojver & Ivancevic, 2011).

## 4.2  Breakdown of a typical UAV structure

This chapter will estimate the impact velocity above which penetration of the aircraft's metal skin can be expected (*ballistic limit*). Due to the complexity of the typical UAV airframe, only the impact of selected UAV components will be modelled.

Currently, the most common UAV type on the market, and which is easily custom made by hobbyist, is the quad copter type UAV (Figure 7). Its airframe consists of an even number of arms holding electrical motors at their ends. The controller, battery and payload are positioned at the hub of the arms. The collision behaviour is complex and depends on the strength, frangibility, relative orientation and mass of the structural elements. A simple analytical model of the whole system is impracticable, and no experimental results exist to create an empirical model. Due to the exposed location of the single components (motors, battery pack), it is suggested to study only the collision of the most dense and heavy parts. The frame holding these parts is assumed to provide no significant resistance upon impact. This is justified, as frames are often made of aluminium tubes, carbon fibre or plastic plates, or balsa wood. This approach simplifies the analysis by allowing the modelling of the separate components as simple geometric objects, such as cylinders or blocks (see Appendix B for details).

A 'small' and a 'big' quad copter will be used as a case study, representing an UAV with a mass of less than 2kg and 2—5kg, respectively. The densest and heaviest parts, which pose the biggest risk of penetration upon impact, are the motors, battery pack(s) and the camera as a typical payload. Figure 7 shows two typical UAVs and their components. Components that will be modelled in the present study were selected from an online hobby store. Table 1 lists the dimensions and weights. These parts are representative only, and do not necessarily comprise a realistic UAV configuration.

The largest motor in Table 1 ('motor C'), combined with 'battery B' of the big quad-copter, represent a fixed-wing UAV. Due to its size and weight, this motor can be used interchangeably with a combustion engine in fixed-wing UAVs (the manufacturer advertises it as a replacement for a 100cc piston engine).

One limitation of the present approach is the assumed infrangibility of the components, which behave like solid blocks of metal upon impact (the density of the parts is similar to aluminium). The results of the calculation should be regarded as conservative, as the parts would experience strong deformations, and might disintegrate completely upon impact. Particularly, the battery pack consists of single cells held together by tape, which makes it quite flexible. Yet, the close proximity of these cells upon impact, and the resulting combined loads, justify modelling the battery pack as a solid block.

**Figure 7: Typical quad copter UAV configurations. Top left: small machine; top right: big machine; bottom: typical structural elements and payloads.**

| | Item | Model | Geometry | Dimensions [mm] | Weight [g] |
|---|---|---|---|---|---|
| Quad-copter (small) | Motor A | NX-4006-530kv | Cylinder | D=45, L=12 | 67 |
| | Battery A | -- | Block | 25x50x65 | 160 |
| | Camera A | GoPro Hero 2 | Block | 42x60x30 | 190 |
| Quad-copter (big) | Motor B | Turnigy Multistar 4830-480Kv | Cylinder | D=47, L=33 | 154 |
| | Battery B | -- | Block | 45x45x138 | 583 |
| | Camera B | Canon EOS 7D | Block | 148x110x74 | 820 |
| Single-engine | Motor C | Turnigy CA120-70 (100cc eq) | Cylinder | D=118, L=120 | 2730 |

**Table 1: Dimensions and weights of representative UAV components.**

## 4.3 Modelling the penetration of plates

### 4.3.1 The ballistic limit

Whether a compact impactor penetrates a flat plate, depends on a series of physical and geometrical parameters, which will be introduced in 4.3.2. The relationship between these parameters has been studied extensively in three fields of application:

A. Ballistic weapon projectiles penetration into steel/armour plates (Goldsmith, 1999)
B. Aircraft collision with debris generated from orbital missile explosions (RCC, 2007)
C. Uncontained engine failure with debris penetration of the aircraft fuselage (Lundin, 2002)

Common to all three examples is the relatively high velocity range, with velocities over 1000ft/s (>590kts) in application A, 700-800ft/s (415—470kts) in B, and 300—800ft/s (177—470kts) in C. The present report will use methods and models from application C, which deals explicitly with aircraft materials (aviation-grade aluminium) and has experimental and numerical data at impact velocities as low as 150ft/s (90kts).

Beginning 2000, the FAA commissioned an extensive experimental study on the consequences of uncontained engine failure, the Uncontained Engine Debris Mitigation Program: UEDMP (Lundin, 2001) (Lundin, 2002). The study examined the impact of turbine engine blade fragments into the fuselage. Of interest for the present report is the estimation of the *ballistic limit* velocity $V_{50}$, which is classically defined as the velocity with a 50% probability of penetration.

Intuitively, the mass of the impacting object and the plate thickness will be among the variables determining the ballistic limit. Figure 8 shows experimental results of the impact of a 1/2" steel sphere into 1/16", 1/8" and 1/4" thick aluminium plates. It can be seen that above a certain impact velocity the residual velocity of the impactor is larger than zero, meaning the impactor has penetrated the plate. The velocity, at which the data points raise for the first time above the horizontal, is the ballistic limit $V_{50}$. As expected, thicker plates require higher velocities for penetration. The higher the impact velocity of the impactor, the higher the residual velocity of the projectile exiting the rear side of the plate will be.
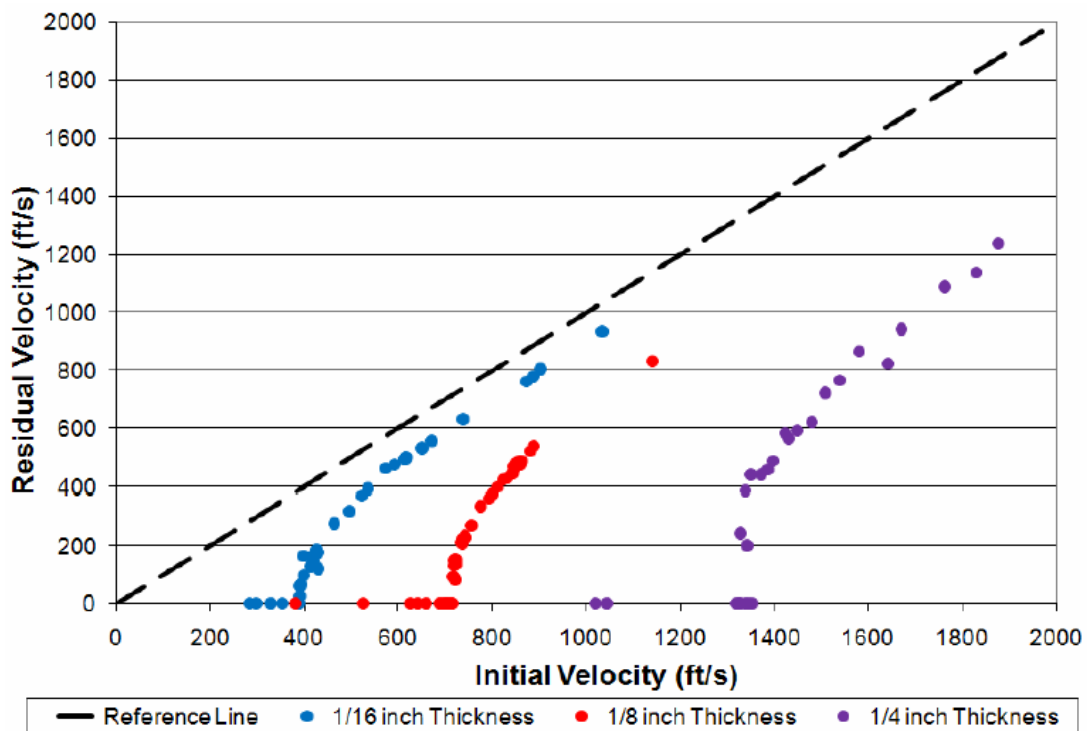


Figure 8: Experimental ballistic limit evaluation for aircraft aluminium plates at different target material thicknesses. The impactor is a 1/2" diameter steel sphere. From (Buyuk, et al., 2008).

### 4.3.2  The FAA penetration equation

The FAA penetration equation will be used for the prediction of the ballistic limit $V_{50}$. This equation is based on the energy required to punch a round hole in a sheet of metal. More details on the assumptions and limitations can be found in Appendix A. The equation is defined as:

$$V_{50} = \sqrt{\frac{2LC_S t^2}{m \cos^2 \theta}}$$

where

- $m$ = the mass of the projectile [kg]
- $\theta$ = the obliquity [radians]; see Figure 9
- $C_S$ = an empirically determined shear constant [Pa], which is roughly correlated with classical material properties
- $L$ = the perimeter of the subtended presented area of the projectile [m]: in the case of impacts with obliquity this is the area of the projectile normal to the velocity at impact and projected onto the target (e.g. roughly the perimeter of the hole in the target)
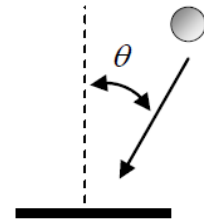- $t$ = the thickness of the target material [m].



Figure 9: Geometry of the oblique impact.

$V_{50}$ is classically defined as the velocity where there is a 50% probability of penetration. However, the FAA penetration equation is deterministic and intended to provide a conservative estimate such that no penetration is predicted for impacts at velocities less than $V_{50}$, and penetration is predicted for impact velocities greater than $V_{50}$.

A *boxplot* will be used in this report to depict the ballistic limit. This representation expresses the probabilistic nature of the impactor orientation relative to the impact plate. The impact area perimeter shows a certain probability distribution, from the least likely (usually the head-on impact with the smallest area) to the largest impact area. The calculation of the probabilities, and an explanation of the boxplot, can be found in Appendix A—C.

## 4.4  Impact: Fuselage and wings

The consequences of aircraft skin penetration by UAV parts will depend on the impact location, and can lead to damage of electrical or hydraulical systems or other control systems, penetration of the fuel tank, weakening of the structural elements (stringers, spars) or injury/fatality of crew members or passengers.

### 4.4.1  Penetration: Fuselage and wings

The fuselage skin is modelled as 1/8" and 1/16" thick aluminium plates ($C_S$=276MPa), under a perpendicular impact. To put the values of $V_{50}$ in perspective, the maximum velocity with fully extended flaps of a Being 747-400 ($V_{FE}$=180kts) and a Boeing 737-400 ($V_{FE}$=162kts) are plotted for comparison. This is the highest expected velocity of a commercial airliner during landing.

Figure 10 shows the ballistic limits of a 1/8" aluminium plate for components of a small UAV, big UAV and a single engine fixed-wing UAV (compare Table 1). All components of the big UAV, and the battery and camera of the small UAV, are likely to penetrate the aircraft skin at velocities even below $V_{FE}$. The 2.73kg heavy motor of the fixed-wing UAV (motor C) causes a penetration already at 60kts.

Figure 11 shows the ballistic limits for an impact into a 1/16" skin section. All UAV components are likely to penetrate the skin for velocities above 100kts.
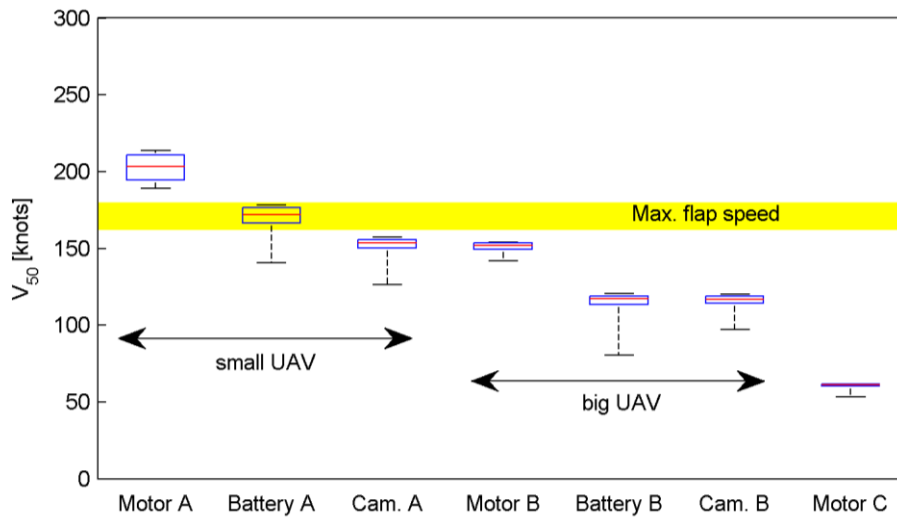


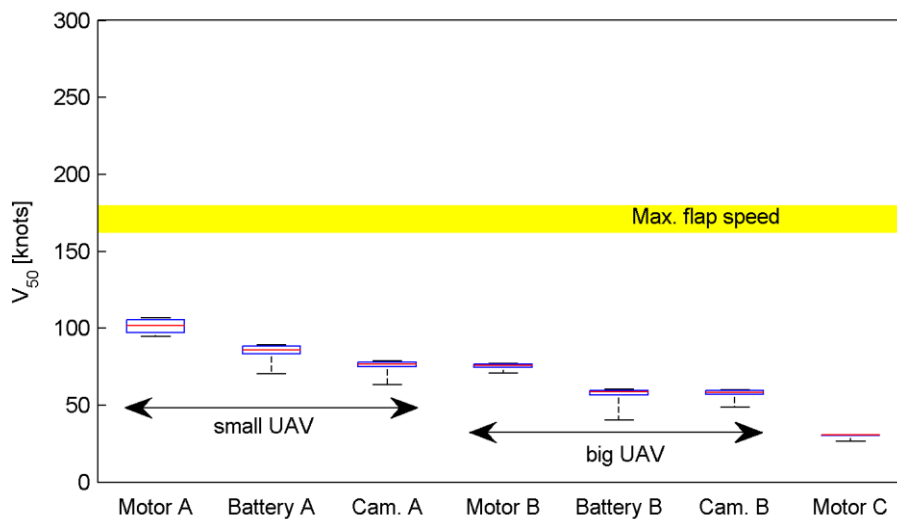**Figure 10: Ballistic limit of 1/8" thick aluminium skin (normal impact).**



**Figure 11: Ballistic limit of 1/16" thick aluminium skin (normal impact).**

## 4.5  Impact: Windscreen

The impact into the windscreen adds two complications:

1. The windscreen is inclined with respect to the flight path.
2. The impact physics of the windscreen material differ from a metal.

### 4.5.1  Validity of the FAA penetration equation

The inclination of the windscreen is taken into account in the FAA equation by the oblique angle θ. There is evidence that the material response to an oblique impact does not follow a simple $\cos\theta$-law (Wilde, 2010), and the FAA equation should be modified to improve its prediction capability. Yet, the large uncertainties introduced by the consideration of a non-metal plate as a target outweigh any gains from the modified equation. The unmodified equation will be used in the present study for simplicity.

The use of a non-metal target material leads to large uncertainties in the results. The FAA equation was developed from and for impacts into metal plates. In particular, the possible change of the failure mechanism is a potential source of error. The empirical constant $C_S$ incorporates the shear strength *and* the failure mechanism ('mode') that occurred during the experiments that the constant was derived from. Two common failure modes are 'petaling' and 'plugging' (Figure 12), in case of thin and thick metal plates, respectively (Buyuk, et al., 2008). When considering a non-metal windscreen, the material's impact resistance is accounted for by substituting $C_S$ with the material's shear strength; yet, this does not take into account a possible change of failure mechanism. The present results for windscreen penetration should be treated as rough estimates with large error bars.
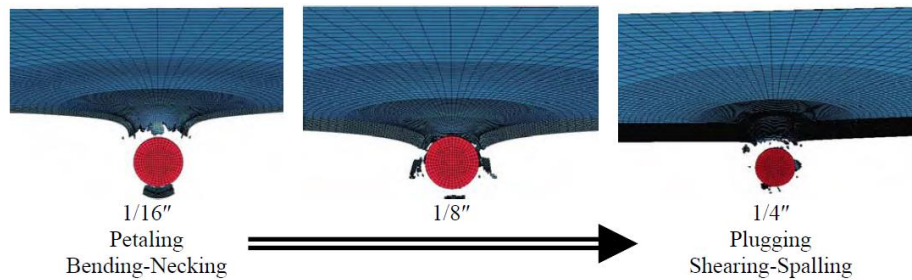


**Figure 12: Transition of failure mode form 'petaling' to 'plugging' depending on plate thickness.**

To make things more complex, the windscreen is usually a multilayer construction of glass and vinyl, resulting in a combination of brittle and elastic behaviour. No experimental data could be found on the impact behaviour (e.g. shear strength) of such composite materials. Some literature suggests modelling the windscreen as a 1/2" thick Lexan, cast acrylic, stretched acrylic, or bullet resistant glass plate (Cole, et al., 1997), while others assume the windscreen's ballistic resistance to be equivalent to a 1/8" thick aluminium plate (Wilde, 2010). Both options will be compared in the present study: a 1/2" thick Lexan plate and a 1/8" thick aluminium plate, both at 40° incidence. In addition, the windscreen of a GA aircraft will be modelled as a 1/8" thick Lexan plate (Table 2).

|    | Material | Shear strength (ultimate) | Thickness | Notes |
|----|----------|---------------------------|-----------|-------|
| **#1** | Aluminium | 276 MPa | 1/8" | (Wilde, 2010) |
| **#2** | Lexan | 68 MPa[6] | 1/2" | (Cole, et al., 1997) |
| **#3** | Lexan | 68 MPa | 1/8" | GA windscreen |

**Table 2: Material properties of the modelled windscreens.**

### 4.5.2  Penetration: Airliner windscreen

Figure 13 shows the ballistic limits for a windscreen modelled as a 1/8" aluminium plate. Only components of the big UAV (and the exceptionally large fixed-wing motor C) are expected to penetrate the windscreen.

Interestingly, any penetration becomes unlikely when the windscreen is modelled as a 1/2" Lexan plate, as shown in Figure 14 (with the exception of motor C). The decreased strength of Lexan is more than balanced by the four-fold increase in plate thickness, compared to the aluminium model. This discrepancy makes the prediction of windscreen penetration ambiguous. It is recommended to accept the more conservative results of Figure 13.

---

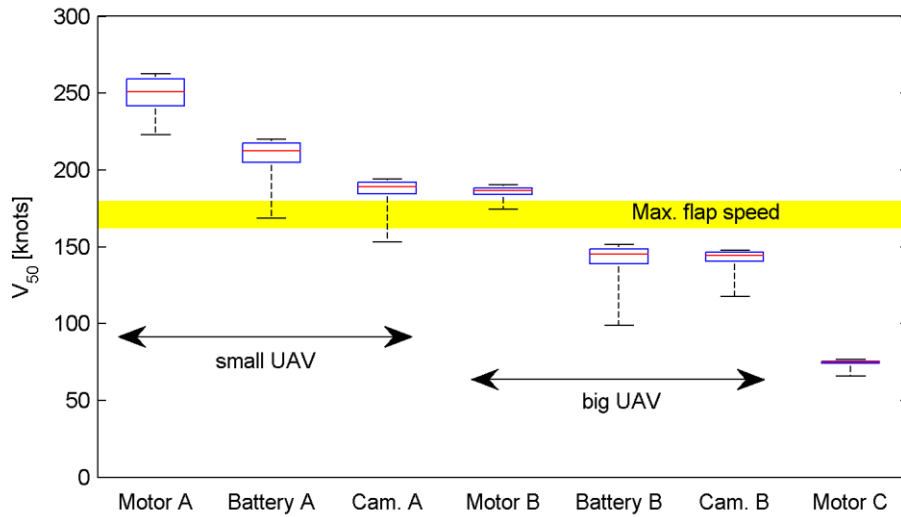[6] http://www.associatedplastics.com/forms/pc_lexan_9034.pdf

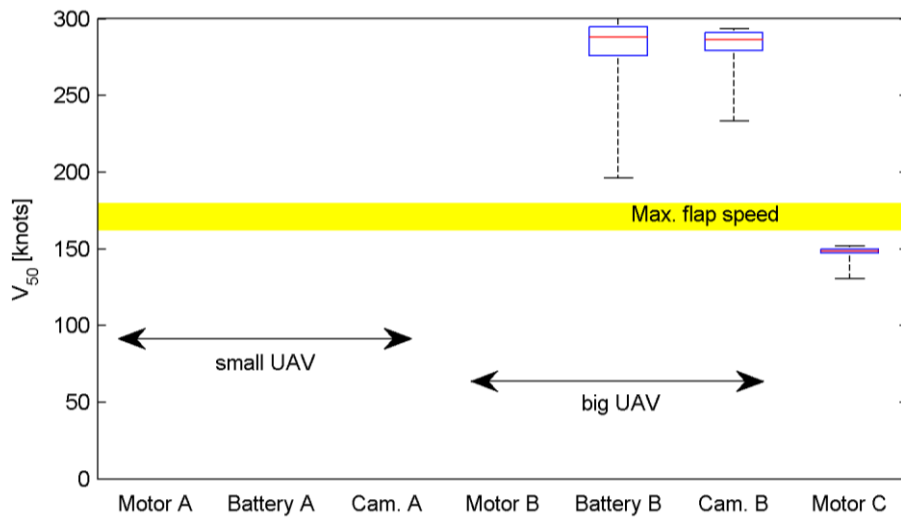**Figure 13: Ballistic limit of the airliner windscreen (40° inclination), modelled as a 1/8" aluminium plate.**



**Figure 14: Ballistic limit of the airliner windscreen (40° inclination), modelled as a 1/2" Lexan plate.**

### 4.5.3 Penetration: General aviation windscreen

The ballistic limits for the penetration of a GA windscreen (1/8" Lexan) are compared to the maximum cruise speed $V_C$ (124kts), and maximum flaps extended speed $V_{FE}$ (87kts) of a Cessna Skyhawk[7]. Figure 15 shows that windscreen penetration can be expected in all cases at cruise speed. In landing configuration ($V_{FE}$), only components of the big UAV (and motor C) are likely to penetrate the windscreen.
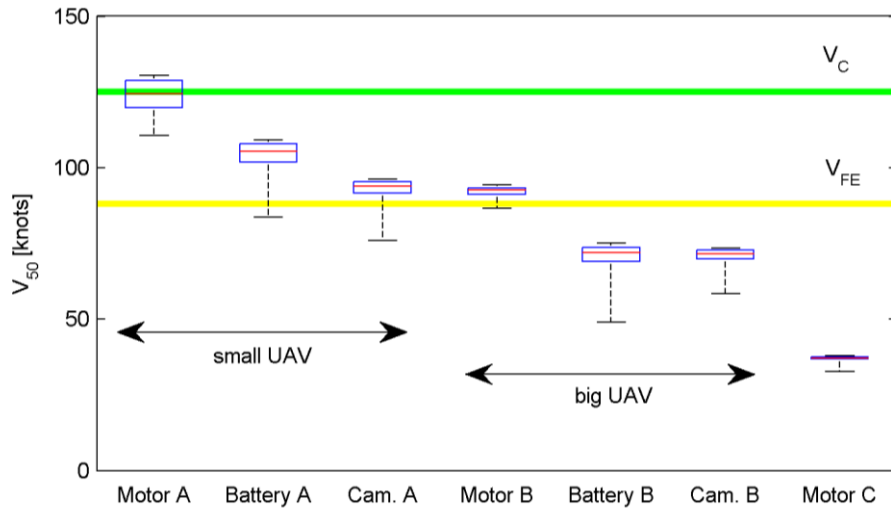


**Figure 15: Ballistic limit of a GA windscreen, modelled as a 1/8" Lexan plate (40° inclination). $V_C$ is the maximum cruise speed and $V_{FE}$ is the maximum flaps extended speed of a Cessna Skyhawk.**

---

[7] http://www.cessna.com/single-engine/skyhawk

# 5  Summary of results

## 5.1  Commercial aircraft: Engine ingestion

1.  3 out of 4 collisions are expected to result in ingestion of the UAV into one of the engines.
2.  The loss of the engine should be assumed, with possible blade fragment throw.
3.  UAV ingestion is very unlikely to result in a catastrophic outcome.

## 5.2  Commercial aircraft: Airframe

1.  For a typical airframe aluminium skin (thickness: 1/8"—1/16"), penetration is predicted for velocities above 200kts, independent of UAV size (the lightest impactor weighing 67g).
2.  During approach with fully extended flaps (at $V_{FE}$=160—180kts), penetration is predicted for a big UAV, and is very likely for a small UAV.
3.  A single engine, fixed-wing UAV is predicted to penetrate the aluminium skin at velocities as low as 40—60kts.

## 5.3  Commercial aircraft: Windscreen

1.  The results strongly depend on the material properties used in the model. The windscreen is likely to tolerate the impact of a small UAV without penetration at $V_{FE}$.
2.  The likelihood of penetration from the impact of a big UAV remains unclear.
3.  A fixed-wing UAV is predicted to penetrate the windscreen at velocities below $V_{FE}$.
4.  The inclination of the windscreen reduces the normal forces, resulting in a higher impact resistance compared to the normal impact into the metal skin.

## 5.4  General aviation aircraft: Windscreen

1.  Penetration is predicted at maximum cruise velocity ($V_C$=124kts for a Cessna 172), independent of UAV size.
2.  Penetration is predicted for a big UAV at $V_{FE}$ (87kts).
3.  Penetration is unlikely for a small UAV at $V_{FE}$.

## 5.5  Conclusions

- A mid-air collision between a commercial airliner and an UAV is most likely to result in the ingestion of the UAV into one of the engines (3 out of 4 events). Reduction or loss of engine thrust with potential debris throw must be assumed. From past experience, engine loss and uncontained engine failure can be regarded as non-catastrophic events.
- A mid-air collision at impact velocities above 200kts is predicted to result in airframe skin penetration, independent of the UAV size. The consequences of such penetration will depend on the impact location.
- During the landing approach (at or below $V_{FE}$=160—180kts), a collision with a large UAV is likely to lead to skin and windshield penetration of a commercial airliner.
- A general aviation windscreen will be penetrated at cruise velocity. During approach (at or below $V_{FE}$=87kts), a large UAV will penetrate the windscreen; a small UAV is likely to be deflected without penetration.
- No experimental data exist to validate the predictions of windscreen penetration by a solid object. It is recommended to commission an experimental study, impacting actual UAV parts into common windscreen materials. Until then, the results presented in this report should be treated as rough estimates.

# 6 Appendix

## A. The FAA penetration equation

The FAA penetration equation is based on the energy required to punch a round hole in a sheet of metal. It has been shown to give accurate, and conservative (Buyuk, et al., 2008) predictions during turbine fragment penetration tests (Lundin, 2001) (Lundin, 2002), and has been applied in a modified form in other studies (Wilde, 2010). The equation uses a combination of physics, an empirically derived constant $C_S$, and the following two assumptions:

1) The minimum energy required for penetration is equivalent to the energy required to shear out a "plug" of the impacted material, as illustrated in Figure 16.
2) The normal component of the impact velocity is the only source of kinetic energy relevant to the minimum energy required for penetration.
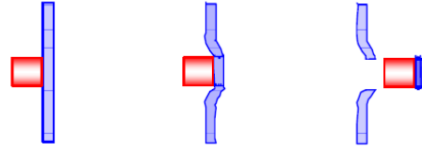
Figure 16: "Plug" penetration of a plate.

These assumptions lead to the following equation:

$$\frac{1}{2}m(V_{50}\cos\theta)^2 = C_s L t^2,$$

where the left hand side represents the kinetic energy of the projectile normal to the plate and the right hand side represents the mechanical work necessary to shear out a plug of the target material. Thus, the FAA equation for the ballistic limit $V_{50}$ is:

$$V_{50} = \sqrt{\frac{2LC_S t^2}{m\cos^2\theta}}$$

where

- $m$ = the mass of the projectile [kg]
- $\theta$ = the obliquity [radians]; see Figure 9
- $C_S$ = an empirically determined shear constant [Pa], which is roughly correlated with classical material properties
- $L$ = the perimeter of the subtended presented area of the projectile [m]: in the case of impacts with obliquity this is the area of the projectile normal to the velocity at impact and projected onto the target (e.g. roughly the perimeter of the hole in the target)
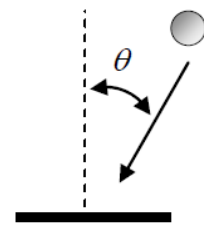- $t$ = the thickness of the target material [m].

Figure 17: Geometry of the oblique impact.

$V_{50}$ is classically defined as the velocity where there is a 50% probability of penetration. Further details can be found in (Wilde, 2010). There are two major difficulties in applying the FAA equation:

The material properties of the target are combined in the shear constant $C_S$. This constant was determined empirically from ballistic impact tests on Aluminium and steel plates (Gunderson, 1977), which theoretically limits the applicability of this equation to these two materials. On the other hand, it has been noted by (Wilde, 2010) that this constant roughly correlates with classical material properties. This implies that the material's shear strength (sometimes referred to as 'Static Yield

Limit') can be used as a good approximation for $C_S$; for aluminium: 210—290MPa, depending on the alloy. This fact was applied in this report for impacts into Lexan windscreens; the shear strength of Lexan was used for $C_S$.

The second difficulty lies in calculation of the impact area perimeter. The underlying assumption of the FAA equation is that certain energy is required to shear out a plug along the perimeter of the impact area. The longer this shear line in the material is, the more shearing energy is needed. It is obvious, that the orientation of the impactor relative to the target plate will determine the impact area and perimeter. Figure 18 shows the presented area $A_P$ of an irregularly shaped object onto a surface perpendicular to the flight path. To calculate the shear line in the target plate which is oblique to the flight path vector, the area $A_P$ must be projected on the inclined surface and its perimeter calculated.



Figure 18: Presented area along the flight path.

This requires the prior knowledge of the impactor orientation and its flight path (impact velocity vector) relative to the target plate.
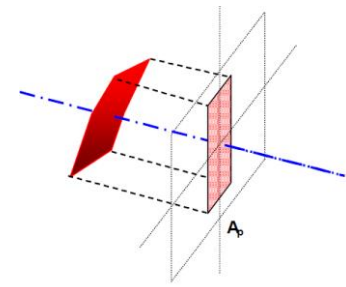
In the present study, the orientation of the impacting UAV parts relative to the aircraft surface is not known. One possibility would be to assume the worst-case (smallest impact area) and best-case (largest impact area) scenarios. Yet, the associated areas do not have equal probability, and the worst-case scenario is likely to be over-restrictive. To accommodate all possible impact orientations, a probabilistic approach has been chosen, in which a pre-defined impactor geometry (battery, motor…) is rotated about all three axis, and its projection on the target surface is calculated. In case of the windscreen, a 40° inclination of this surface relative to the flight path of the object is added. The perimeter of this projected area is calculated for each impact orientation, which leads to a probability distribution. The results show that the worst-case scenario is the least likely, and that the most probable perimeter is almost twice as large as the smallest. The details of the MatLab simulation can be found in Appendix B.

The distribution of probability for a certain impact perimeter (and the derived ballistic limit $V_{50}$) is represented in form of a boxplot (sometimes called box-and-whiskers plot). A boxplot graphically depicts a set of numerical data through their quartiles (Figure 19). A quartile contains a quarter (25%) of all data points of the set. The upper and lower whisker ends show the maximum/minimum values; the central box combines 50% of all data points. The line in the box shows the median. The boxplot should be interpreted as follows: If the box lies half-way between the whiskers and has approximately the same length as the whiskers combined, then the data is uniformly distributed. Figure 19**Error! Reference source not found.** shows a data set concentrated and skewed to higher values, as the main box is considerably smaller than the whiskers and lies closer to the maximum value. In the present study, this would mean that higher values are more likely; the $V_{50}$ velocity should be expected to lie close the maximum value, and smaller values are less probable.
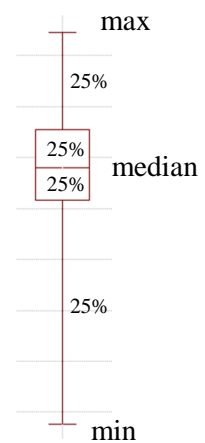


Figure 19: Box plot

The boxplot should not be confused with an error bar plot. The boxplot shows the variability of the result due to only one parameter (impact area perimeter $L$). The errors and uncertainties in the remaining parameters of the FAA equation are not accounted for.

An objection to the probabilistic approach is the fact that UAV components are installed with a 'standard' orientation (motors vertically, battery pack usually horizontally), which makes their orientation pre-determined relative to the horizontal plane during hovering and slow level flight. Nevertheless, such assumptions would limit the scope of impact possibilities and, in particular, exclude the worst-case scenario ('tail-on' impact with the smallest area). The probabilistic approach, on the other hand, provides an overview of the whole range of possibilities, regardless of the design of the particular UAV model.

## B. Monte Carlo simulation

To compute the probability distribution of the impact perimeter $L$ for the FAA equation, surface meshes of two geometric objects were created in MatLab: A square blocks, representing the UAV battery pack and the camera payload; and a cylinder, representing the UAV electric motor (Figure 20). The projection of these surface meshes onto a flat surface (inclined by 40°, in case of the windscreen) provided the impact area and perimeter length. The object was rotated in steps of 8° (45 steps per 360° rotation) about all three axes, resulting in $45^3 = 91125$ projections per object. A histogram of the perimeter lengths for a sample case is shown in Figure 21. The strong skewness of the distribution towards the maximum value implies that a small-area impact (a 'tail-on' collision) is least likely. The cumulative sum (blue line) is used for the calculation of the quartiles and the boxplot. The boxplot reflects the strong skewness towards large perimeters by having the main box and the median located at the right end of the range (see insert in Figure 21).
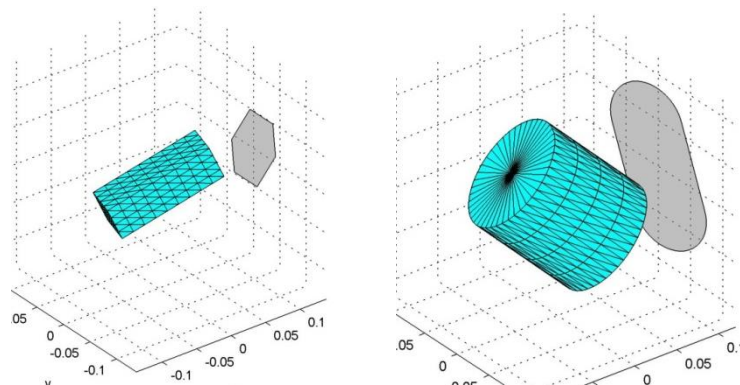


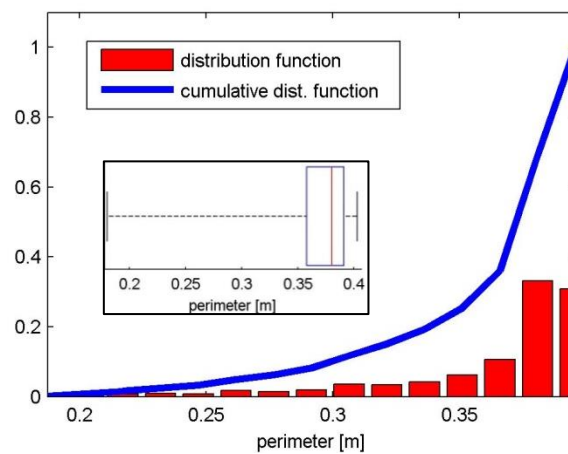Figure 20: 3D mesh and its projection for the battery pack (left) and motor (right).



Figure 21: Impact perimeter distribution for a battery pack (red bars) and the cumulative distribution function (blue line) for the calculation of statistics. The resulting boxplot is shown in the insert. The data show a strong skewness to large impact perimeters, making 'tail-on' collisions least likely.

## C. Mathematical discussion of probability

The three-dimensional object impacting an inclined surface is a very complex problem for an analytical probabilistic treatment. The underlying mathematical principles can be explored analytically when this three degrees of freedom problem (3DOF) is reduced to a 1DOF situation.

The simplest problem to consider is the projection of a unit line (length=1) onto a wall perpendicular to the horizontal axis, as shown in Figure 22. The line is fully determined by only one parameter, the angle $\alpha$. The length of the projection will be termed $X$, with:
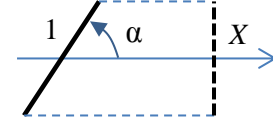


$$X = |\sin \alpha|$$

$X$ is periodic with $\alpha$, and the full range of results is reproduced within $0 \le \alpha \le \pi/2$ ($0 \le \alpha \le 90°$). When considering probabilities, we can say that the continuous *sample space $\Omega$* consists of lines of lengths between 0 and 1, with $X$ being the *continuous random variable*, which describes the outcome of a random experiment (Grinstead & Snell, n.d.). The 'experiments' consist of picking $\alpha$ randomly between 0 and $\pi/2$ many times, and calculating $X$. The result is a distribution of probabilities for a certain outcome. This can be represented in form of the *cumulative distribution function $F(x)$*, which describes the probability $P$ that the outcome $X$ will lie below a given value $x$ (in this case $0 \le x \le 1$):

$$F(x) = P(X \le x)$$

With $X = \sin \alpha$, we can write:

$$F(x) = P(\sin \alpha \le x)$$
$$= P(\alpha \le \sin^{-1} x)$$
$$F(x) = \frac{2}{\pi} \sin^{-1} x$$

The step leading to the last equation can be understood from Figure 23: The probability for $\alpha \le \sin^{-1} x$ at a given $x_i$ is equivalent to the ratio of the red to green lines.
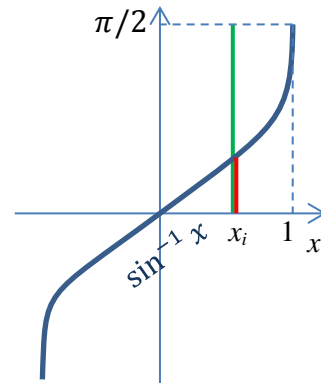
The *probability density function $f(x)$* is computed as:

$$f(x) = \frac{dF(x)}{dx} = \frac{2/\pi}{\sqrt{1 - x^2}}$$

These functions are plotted in Figure 24, which shows that the probability density is far from uniform, and is concentrated at larger values of $x$. This means that it is more likely to encounter values close to 1 than to 0. This is quantified by the quartiles (0.25, 0.5, 0.75) plotted as crosses in Figure 24, with the larger cross representing the median of the distribution. The median lies at 0.707, meaning that in 50% of all 'experiments', the length $X$ will lie below this value, and in 50% above. Low values of $X$ are less likely: for example, the probability of encountering the smallest 10% of all projection lengths is only 6.3%, compared to a probability of 28.7% for the highest 10%.
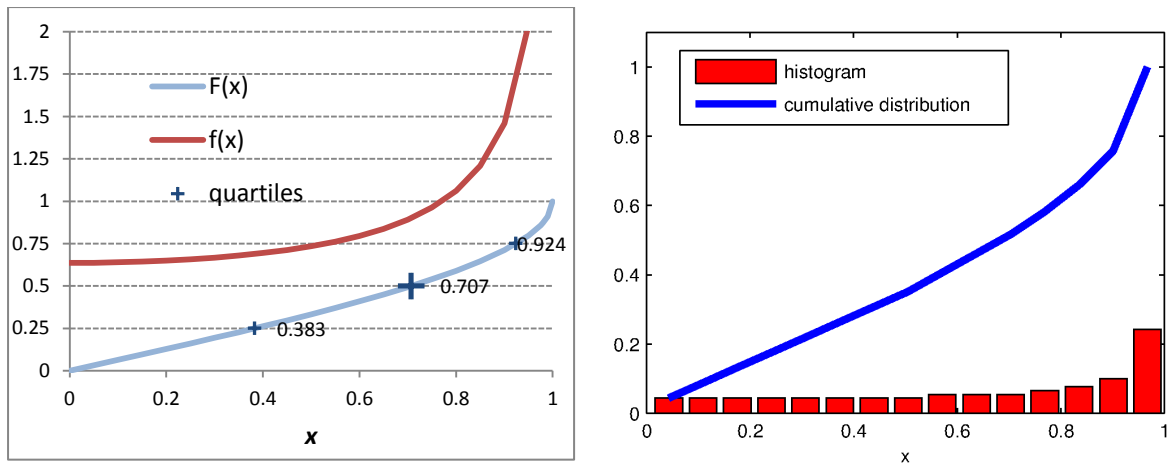
**Figure 24: Cumulative distribution function F(x) and probability density function f(x) of the projection length. Left: Analytical solution; right: MatLab simulation.**

This probability distribution explains why it is so difficult to make a knife stick with its pointy end in a soft target by throwing it with a spin. As it has been shown, it is more likely that it will impact with its long side than with its pointy end.

When transferring these results to the 3DOF case of an elongated three-dimensional object impacting the windscreen, it is apparent that the impactor is more likely to present a large impact area/perimeter. The worst-case scenario, the object impacting with its smallest surface, is less likely.

# 7 Bibliography

ATKINS, 2008. *Bird Strike Damage & Windshield Bird Strike - Final Report,* s.l.: European Aviation Safety Agency.

Buyuk, M., Loikkanen, M. & Kan, C.-D., 2008. *Explicit Finite Element Analysis of 2024-T3/T351 Aluminum Material Under Impact Loading for Airplane Engine Containment and Fragment Shielding,* Washington, DC: U.S. Department of Transportation (Federal Aviation Administration).

Cleary, E. C., Dolbeer, R. A. & Wright, S. E., 2006. *Wildlife Strikes to Civil Aircraft in the United States 1990-2005,* s.l.: Bird Strike Committee.

Cole, K. J., Young, L. W. & Jordan-Culler, T., 1997. *Hazards of Falling Debris to People, Aircraft, and Watercraft,* Albuquerque, New Mexico: Sandia National Laboratories.

Draper, C. H. & Wilde, P. D., 2008. *Development of a Business Jet Class Survivability Model for.* Honolulu, Hawaii, AIAA 2008-7122.

Goldsmith, W., 1999. Non-ideal projectile impact on targets. *International Journal of Impact Engineering,* Volume 22, pp. 95-395.

Grinstead, C. M. & Snell, L. J., n.d. *Introduction to Probability.* 2nd ed. s.l.:American Mathematical Society.

Gunderson, C., 1977. *Study to improve airframe turbine engine rotor blade containment,* s.l.: U.S. Department of Transportation.

Lundin, S., 2001. *Engine Debris Fuselage Penetration Testing Phase I,* s.l.: U.S. Department of Transportation.

Lundin, S., 2002. *Engine Debris Fuselage Penetration Testing Phase II,* s.l.: U.S. Department of Transportation.

RCC, 2007. *Common Risk Criteria Standards for National Test Rdanges: Supplement,* New Mexico: Range Commanders Council, U.S. Army White Sands Missile Range.

Smojver, I. & Ivancevic, D., 2011. Bird strike damage analysis in aircraft structures using Abaqus/Explicit and coupled rian Lagrangian approach. *Composites Science and Technology,* Volume 71, p. 489–498.

Thorpe, J., 2012. *100 years of fatalities and destroyed civil aircraft due to bird strikes.* Stavanger, Norway, International Bird Strike Committee 30/WP.

Vignjevic, R., Olowski, M., De Vuyst, T. & Campbell, J. C., 2013. A parametric study of bird strike on engine blades. *International Journal of Impact Engineering,* Volume 60, pp. 44-57.

Wilde, P. D., 2010. *Aircraft Protection Standards and Implementation Guidelines for Range Safety.* Orlando, Florida, AIAA 2010-1542.